Role of Trapped Particles and Waves in Plasma Solitons-Theory and Application

Physica Scripta. Vol. 20, 306–316, 1979

Role of Trapped Particles and Waves in Plasma Solitons - Theory and Application

Hans Schamel

Theoretical Physics I, Ruhr-University Bochum, FRG

Received June 7, 1978

Abstract

Role of trapped particles and waves in plasma solitons – theory and application. Hans Schamel (Theoretical Physics I, Ruhr-University Bochum, FRG).
Physica Scripta (Sweden) 20, 306–316, 1979.

In this tutorial and review paper, we investigate the influence of trapped particles on the propagation of ion acoustic solitons and the role of trapped waves on the propagation of Langmuir solitons. The classical potential method allows us to construct finite amplitude soliton solutions, and trapping phenomena are found to retard the motion of solitons. Thus, ion acoustic solitons have minimum speed when they are based on an isothermal electron equation of state since this corresponds to "maximum electron trapping". In the small amplitude regime, deviations from the Boltzmann law lead to a new nonlinear term. Subsequently, the dynamics of the soliton is governed by a modified KdV-equation [e.g., (23)]. For Langmuir solitons an existence diagram is found and exhibits the comparison between experimentally observed localized structures and theory. The connection with the various small amplitude soliton solutions is also pointed out. Moreover, the inclusion of a pump and of dissipative terms in the coupled nonlinear Schrödinger-ion equation gives rise to a transient phenomenon called soliton flash, whose implication to the laboratory experiments is discussed. Finally, as an application in numerical analysis the propagation of solitons is followed by solving the KdV-equation in Fourier-space. This turns out to be an excellent tool to test stability and accuracy of numerical schemes. Our results reveal that the so-called aliasing interactions lead to erroneous solutions. The conservation of invariants does not guarantee the accuracy of a numerical algorithm, although it is needed for its stability.

1. Introduction

The theory of solitons (solitary waves) has received special attention in the past decade mainly due to two facts: Firstly, solitons appear in many fields of our life ranging from classical fluids, solid state and elementary particle physics to biophysics as reflected in the articles published in this volume. Secondly, it was the soliton theory from which a new branch in mathematics originated, namely, the inverse scattering method to solve initial value problems. These rapidly developing fields with many applications in science are by no means exhausted at the present time, despite a large number of papers already published. Several excellent monographs [1–4] provide a profound insight into the nature of this nonlinear phenomenon and review the present state of art.

Physically, single humped waves exist due to the balance between nonlinear steepening and dispersive spreading of the wavepackets, propagating in a weakly dispersive medium. They are termed solitons because their shape and speed are preserved after a collision. From a mathematical point of view the analysis of classical solitons is usually based on the Korteweg–de Vries equation (or on analogous equations like the nonlinear Schrödinger-equation for the case of envelope solitons) which is derived from basic equations by means of a small amplitude expansion.

In the present paper we avoid this restriction. The price is a loss of flexibility with respect to temporal and spatial changes. A fully nonlinear analysis demands almost necessarily the use of a steady state and of a homogeneous unperturbed medium. The advantage of taking the nonlinear behaviour into account completely is a broader range of applicability, when compared with experimental and numerical measurements. A fully nonlinear theory also provides a standard for checking approximations, made in a more involved analysis.

This article is, therefore, devoted mainly to stationary solitons and the study of trapping effects related with them. This includes particle trapping in ion acoustic solitons (Section 2) and field trapping in Langmuir solitons (Section 3) as well. Comparisons with experiments are made and possible applications are discussed. Deviating from the main line, we also study a more transient phenomenon called soliton flash because of its practical importance in laser fusion, and mention numerical schemes to solve nonlinear wave equations (Section 4).

2. Particle trapping in ion acoustic solitons

2.1. *Finite amplitude solitons*

In this section, we investigate finite amplitude soliton solutions and study the effect of trapped particles by means of the "classical potential method".

The basic equations we solve are

$$\frac{\partial}{\partial t} n_i + \frac{\partial}{\partial x} n_i u_i = 0 \qquad \text{(continuity)} \qquad (1a)$$

$$\frac{\partial}{\partial t} u_i + u_i \frac{\partial}{\partial x} u_i = -\frac{\partial}{\partial x} \phi \qquad \text{(Euler)} \qquad (1b)$$

$$\frac{\partial^2}{\partial x^2} \phi = n_e - n_i \qquad \text{(Poisson)} \qquad (1c)$$

$$0 = \frac{\partial \phi}{\partial x} - \frac{1}{n_e} \frac{\partial}{\partial x} p_e \qquad \text{(force balance)} \qquad (1d)$$

where the notation is standard. The dependent and independent quantities, $t, x, u_i, n_i, n_e, \phi$ and p_e are normalized by the reciprocal ion plasma frequency ω_{pi}^{-1}, the Debye length $\lambda_D = (kT_e/4\pi n_0 e^2)^{1/2}$, the ion sound speed $c_s = (kT_e/m_i)^{1/2}$, the unperturbed density n_0, kT_e/e and $n_0 kT_e$, respectively. In the hydrodynamic equation for the ions we have neglected the ion pressure term and the electrons are assumed to be inertialess.

Equation (1d) is satisfied by an electron equation of the form $p_e = p_e(\phi)$ (rather than $p_e = p_e(n_e)$), which is related to the electron density by

$$\frac{dp_e}{d\phi} = n_e(\phi) \qquad (2)$$

Note that the electron trapping effects enter through $n_e(\phi)$. The

latter follows from the stationary Vlasov equation as shown later. Now we look for stationary wave solutions and transform the system into the wave frame by a Galilei transformation $(x, t, u \to x - Mt, t, u - M)$, M is the Mach-number or normalized wave velocity. Integrating the first two equations, we get

$$n_i u_i = -M \tag{3a}$$

$$u_i^2/2 + \phi = M^2/2 \tag{3b}$$

where we assumed an unperturbed state at infinity ($n = 1, \phi = 0$ $u = -M$) corresponding to localized perturbations. From (3a, b) it follows that

$$u_i = -(M^2 - 2\phi)^{1/2} \tag{4a}$$

$$n_i = (1 - 2\phi/M^2)^{-1/2} \tag{4b}$$

showing that the ion velocity decreases and the density increases with increasing ϕ. The applicability of the present analysis demands that

$$2\phi/M^2 < 1. \tag{5}$$

Knowing n_e, n_i as functions of ϕ, we can integrate Poisson's equation (1c) once, and find

$$\phi'(x)^2/2 + V(\phi) = 0 \tag{6}$$

where $V(\phi)$ is given by

$$V(\phi) = 1 - p_e(\phi) + M^2[1 - (1 - 2\phi/M^2)^{1/2}] \tag{7}$$

The integration constant has been chosen such that $V(0) = 0$. Equation (6) is analogous to the energy equation of a classical particle, $V(\phi)$ representing the potential energy. Stationary wave solutions are obtainable if a second zero of V denoted by ψ, i.e., $V(\psi) = 0$, exists besides $\phi = 0$, and if V is negative in the interval $0 < \phi < \psi$. ψ is the amplitude of the wave whose spatial dependence is entirely determined by $V(\phi)$. The existence condition $V(\psi) = 0$ is nothing else but the nonlinear *dispersion relation* relating the phase velocity or Mach-number M of the wave with its amplitude ψ. We obtain

$$M^2 = \frac{[p_e(\psi) - 1]^2}{2[p_e(\psi) - 1 - \psi]} \tag{8}$$

Hence, the Mach-number of the wave is affected by the electron equation of state. At the "turning points" $V(\phi)$ behaves like

$$V(\phi) = \begin{cases} [M^{-2} - n_e'(0)]\phi^2/2 & 0 \leqslant \phi \ll 1 \\ [n_e(\psi) - (1 - 2\psi/M^2)^{-1/2}](\psi - \phi) & 0 \leqslant \psi - \phi \ll 1 \end{cases} \quad \text{for} \tag{9}$$

From the above we see that the solution is of soliton-type, provided the expressions in the square brackets are negative. To be more specific we now construct appropriate electron pressure laws and densities.

Since the temporal change of the plasma quantities during the passage of the wave occurs on the ion plasma period ω_{pi}^{-1}, the electron quantities being affected on the shorter ω_{pe}^{-1}-timescale, can be considered as quasi-stationary. To get solutions of the stationary Vlasov equation we have to distinguish between free and trapped electrons. Their range is given by the constant of motion $E = v^2/2 - \phi$ where the electron velocity v is now normalized by the electron thermal speed $(kT_e/m_e)^{1/2}$. Particles are free (trapped) if their total energy $E > 0$ ($E \leqslant 0$). In principle, two distribution functions can be described independently [5]

$$f_e(x, v) = \begin{cases} f_{oe}(\xi) & E > 0 \\ f_{et}(\xi) & E \leqslant 0 \end{cases} \tag{10}$$

where $\xi = (2|E|)^{1/2}\ \mathrm{sgn}\ v$. However, as shown in [6], the freedom in choosing f_{oe}, f_{et} must be restricted if we demand that with vanishing amplitude the nonlinear solution approaches a familiar linear wave solution which is in the present case the ion acoustic wave solution. There are two requirements which must be fulfilled

$$f_{et}(0) = f_{oe}(0) \tag{11a}$$

$$f_{et}'(0) = 0 \tag{11b}$$

expressing the fact that at the transition point between free and trapped particles the distribution function must be continuous (11a), and the slope of the trapped electron distribution function in the velocity space must be finite (11b).

Both requirements are satisfied if we choose Maxwellians

$$f_{oe}(\xi) = (2\pi)^{-1/2} \exp[-\xi^2/2] \tag{12a}$$

$$f_{et}(\xi) = (2\pi)^{-1/2} \exp[-\beta\xi^2/2] \tag{12b}$$

The introduction of the parameter β allows for a different temperature in the Maxwellian for the trapped electrons, $\beta = 0$ corresponding to a flat-topped electron distribution. Note, that a hole in the trapped region, corresponding to an underpopulation of trapped electrons, is represented by negative β's.

With these distributions we get [7]

$$n_e(\phi) = \int_{-\infty}^{+\infty} f_e(x, v)\, dv = \exp(\phi)\,\mathrm{erfc}(\phi^{1/2}) + |\beta|^{-1/2} \begin{cases} \exp(\beta\phi)\,\mathrm{erf}[(\beta\phi)^{1/2}] & \beta \geqslant 0 \\ (2/\pi^{1/2})W[(-\beta\phi)^{1/2}] & \beta < 0 \end{cases} \tag{13}$$

and for the electron equation of state we readily obtain

$$p_e(\phi) = 1 + \int_0^{\phi} n_e(\phi)\, d\phi = \exp(\phi)\,\mathrm{erfc}(\phi^{1/2}) + 2(1 - \beta^{-1})\left(\frac{\phi}{\pi}\right)^{1/2} + \frac{1}{\beta|\beta|^{1/2}} \begin{cases} \exp(\beta\phi)\,\mathrm{erf}[(\beta\phi)^{1/2}] & \beta \geqslant 0 \\ (2/\pi^{1/2})W[(-\beta\phi)^{1/2}] & \beta < 0 \end{cases} \tag{14}$$

where $W(x)$ is the Dawson integral.

This general law includes the two equations of states known in the literature, namely,

(i) the isothermal equation of state ($\beta = 1$) [8]

$$p_e(\phi) = \exp(\phi) \tag{15a}$$

(ii) the state for flat-topped distributions ($\beta = 0$) [9]

$$p_e(\phi) = \exp(\phi)\,\mathrm{erfc}(\phi^{1/2}) + 2(1 + 2\phi/3)(\phi/\pi)^{1/2} \tag{15b}$$

the latter often erroneously referred to as "maximum-density-trapping". Figure 1 shows the amplitude dependence of the Mach-number equation (8), plotted for both equations of state (15a, b). A flattened electron distribution carrying a smaller amount of trapped electrons gives rise to a higher Mach-number. The maximum velocity given by the wave breaking condition $M = (2\psi)^{1/2}$ [see eq. (5)] increases from $M = 1.59$ ($\psi = 1.26$) for $\beta = 1$ to $M = 3.1$ ($\psi = 4.8$) for $\beta = 0$, and still higher Mach-numbers are accessible if β is further decreased. It follows that trapped electrons introduce some kind of inertia on the propagating wave.

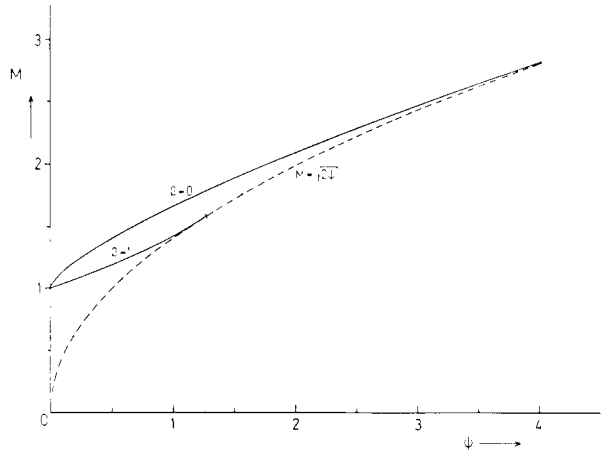

Fig. 1. Machnumber M versus amplitude ψ, $\beta = 1$ corresponds to the isothermal equation of state for the electrons whereas $\beta = 0$ represents flat trapped electron distributions. The dashed line marks the wave-breaking condition.

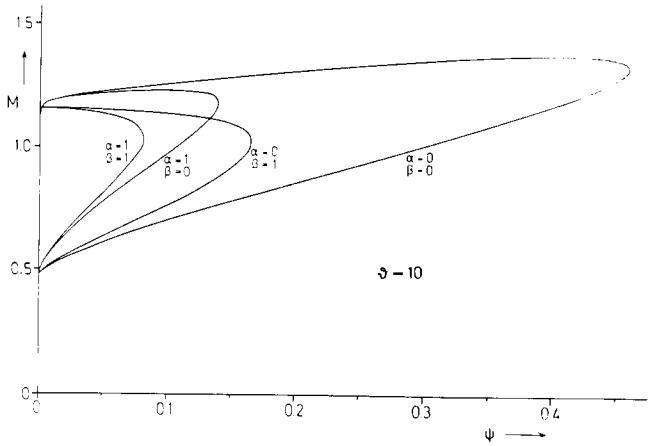

Fig. 3. M vs. ψ for various trapping parameters. α (β) characterizes the trapped ion (electron) distribution. A zero corresponds to a flat distribution for trapped particles, whereas for α (β) equal unity, the trapped particles are described by a Maxwellian, having the same temperature than the untrapped ones.

If finite ion temperature is considered, some of the ions will be trapped, and one should adopt a Vlasov description for the ions, too. We do not bring the analysis here and refer to the original paper [7] for details. Two results are to be noted:

(i) with increasing T_i the range of possible soliton solutions shrinks, below $\vartheta = T_e/T_i < 3.5$ no ion acoustic soliton can propagate (Fig. 2),

(ii) the number of trapped ions, described by α, the analogue to the parameter β, has a relatively strong influence on the M–ψ-relation (Fig. 3). Again, trapped ions hinder the propagation of solitons since M and the maximum ψ increase with decreasing α.

2.2. *The KdV-limit*

In this section we discuss the small amplitude limit and derive an extended KdV-equation.

For small amplitudes, $\psi \ll 1$, the expressions derived above, simplify. By Taylor-expansion of (13) and (14) we get

$$n_e(\phi) = 1 + \phi - \tfrac{4}{3}b\phi^{3/2} + \phi^2/2 + \dots \tag{16a}$$

$$p_e(\phi) = 1 + \phi + \phi^2/2 - \tfrac{8}{15}b\phi^{5/2} + \phi^3/6 + \dots \tag{16b}$$

where

$$b = (1-\beta)\pi^{-1/2} \tag{17}$$

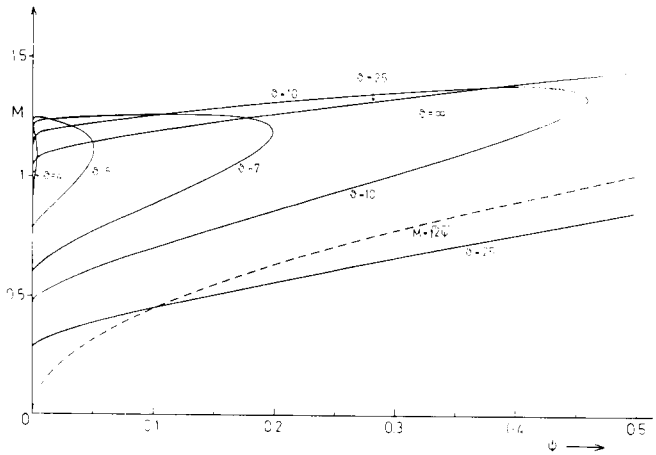

Fig. 2. M vs. ψ for various temperature ratios $\vartheta = T_e/T_i$. The dotted line represents the cold ion limit. For finite ϑ there exists, besides the ion acoustic branch, a second branch which is related with thermal ions [see Stix's textbook (1962), Sections 9–14]. It disappears if $T_i \to 0$, so that no solution exists below the wave-breaking condition $M = (2\psi)^{1/2}$.

Then the Mach-number (8) becomes

$$M^2 = 1 + \tfrac{16}{15}b\psi^{1/2} + [\tfrac{2}{3} + \tfrac{256}{225}b^2]\psi + \dots \tag{18}$$

and the "classical potential energy" (7) can be written as

$$-V(\phi) = \tfrac{8}{15}b\phi^2(\psi^{1/2} - \phi^{1/2}) + \tfrac{1}{3}\phi^2(\psi - \phi) + \dots \tag{19}$$

Integrating (6) with $V(\phi)$, given by (19) yields the generalized soliton solution [7]

$$\phi(x) = \psi\left[1 + \frac{\mathrm{th}^2 y}{1+Q}\right]^{-2} \mathrm{sech}^4 y \tag{20}$$

where $y = (x/2)[(1+Q)\psi/6]^{1/2}$ and $Q = \tfrac{8}{5}b\psi^{-1/2} > -1$. This solution contains the well-known isothermal soliton ($\beta = 1$; $b = Q = 0$)

$$\phi(x) = \psi\,\mathrm{sech}^2[(\psi/6)^{1/2}x] \tag{21a}$$

$$M = 1 + \psi/3. \tag{21b}$$

as well as the soliton solution for nearly flat-topped electron distributions ($|\beta| \ll 1$; $Q \gg 1$)

$$\phi(x) = \psi\,\mathrm{sech}^4\left[\left(\frac{b\psi^{1/2}}{15}\right)^{1/2} x\right] \tag{22a}$$

$$M = 1 + \tfrac{8}{15}b\psi^{1/2} \tag{22b}$$

For a given ψ the second soliton propagates faster than the first one and has a smaller width, confirming again the inertia of the medium due to trapped electrons.

We now present the evolutionary equation to which (20) is a stationary solution. We use the reductive perturbation method to derive the corresponding KdV-equation, and for that reason extend $n_e(\phi)$ in (16a) to

$$n_e(\phi) = 1 + \phi - \tfrac{4}{3}b\phi|\phi|^{1/2} + \phi^2/2 + \dots \tag{16c}$$

and for convenience, assume the third and fourth terms to be of the same order. The absolute sign in (16c) removes the restriction of positive ϕ, and allows the development of a dispersive wave train with negative ϕ. Using the usual stretching of variables [$\xi = \psi^{1/2}(x-t)$; $\tau = \psi^{3/2}t$] we get, from (1a–1c) with (16c) [10]

$$\frac{\partial}{\partial t}\phi + (1 + b|\phi|^{1/2} + \phi)\frac{\partial \phi}{\partial x} + \tfrac{1}{2}\frac{\partial^3 \phi}{\partial x^3} = 0 \tag{23}$$

This KdV-type equation is formulated in the frame where the unperturbed plasma is at rest.

The deviation of the electron equation of state from the isothermal law introduces an additional nonlinearity which dominates if b becomes of order unity. As shown in [10], solitary waves satisfying this equation are preserved after collisions and deserve the notation soliton.

2.3. *Applications*

From the analysis given above it follows that by studying the soliton propagation one can, in principle, infer on the collisionless nature of the electrons and especially on the strength of the diffusion in the trapped electron region. Collisions in the resonance region are unavoidable and, in fact, necessary to establish distributions like (12) [11, 12].

A similar method, the launching of small amplitude test waves, is frequently used to find unperturbed plasma quantities like T_e, n_e, etc. In the present case, the intrinsic nonlinear character of electron trapping demands a propagating nonlinear wave for its investigation.

Non-isothermal equations of states, discussed above, are evident in particle simulations [9, 13–15], in bow shock measurements [16] or in laboratory experiments [17]. However, none of them are directly related to soliton formation. The experiments either deal with ion acoustic shock waves, in which two different asymptotic states are linked, or with the generation of BGK-waves which are periodic rather than solitary-like. {In laminar or weakly turbulent shockwaves where the number of reflected ions (precursor ions) is small, the moving shock-front is usually described by one half of a soliton solution [18].}

On the other hand, the solitons generated by Ikezi and collaborators find an explanation within the usual soliton theory, e.g., as mentioned in [19], the deviation of the Mach-number and soliton width from the isothermal, cold ion prediction (21a, b) found by Ikezi [20] is probably an effect of the finite ion temperature.

This is different to the observations made by Means et al. [21] in connection with shock-experiments, where finite ion temperature corrections to the isothermal M–ψ-law (21b) cannot account for the discrepancy in the relationship $M = 1 + 0.6\psi$ experimentally obtained. A Mach-number, based on the equation of state (15b), $\beta = 0$, together with a distribution of the reflected ions turbulently flattened, was found to fit the experimental curve best. In my opinion, the linear character of their M–ψ relation suggests a less pronounced deviation from the isothermal law and can be described equally well by (18) with $b = 0(\psi^{1/2})$.

Closing this section, we state that a direct verification of this non-isothermal soliton is still lacking but that observations exist which may encourage experimentalists to look for this structure.

3. Field trapping in Langmuir solitons

The second branch of wave solutions in an unmagnetized infinite plasma does not exhibit soliton solutions of the type discussed in the previous section. Langmuir waves are strongly dispersive and cannot be concentrated in a single wave packet for long time. Through wave coupling process, however, they can couple with the slow background plasma motion producing a density cavity which in turn, trap them. This entity is called Langmuir- or envelope soliton and is the subject of this section.

3.1. *Finite amplitude envelope solitons*

First, we discuss the existence of finite amplitude envelope solitons. The appropriate equations are [22], [23]

$$2i\epsilon \frac{\partial}{\partial t} E + 3 \frac{\partial^2}{\partial x^2} E = (n_i - 1)E \tag{24a}$$

$$\frac{\partial}{\partial t} n_i + \frac{\partial}{\partial x}(n_i u_i) = 0 \tag{24b}$$

$$\frac{\partial}{\partial t} u_i + u_i \frac{\partial}{\partial x} u_i = -\frac{\partial}{\partial x}(\ln n_i + |E|^2) \tag{24c}$$

where $\epsilon = (m_e/m_i)^{1/2}$. E represents the slowly varying amplitude of a Langmuir wave-packet and is normalized by $(4\pi n_0 k T_e)^{1/2}$, x, t, n_i, and u_i are normalized as before.

The nonlinear Schrödinger-equation (24a) is derived from the linear wave equation for Langmuir waves which in the dimensional form can be written as

$$3v_{te}^2 \frac{\partial^2}{\partial x^2} E_0 + \omega^2 \epsilon_0 E_0 = 0 \tag{25}$$

Here, $v_{te}^2 = \kappa T_e/m_e$, and ϵ_0 is the cold plasma linear dielectric constant

$$\epsilon_0 = 1 - \omega_{pe}^2/\omega^2 \tag{26}$$

Thereby, the total electric field is given by $E = E_0(x)\, e^{-i\omega t} +$ c.c. If we allow for temporal changes of the amplitude on a slow time scale, we can replace ω^2 in (25) by $[\omega - i(\partial/\partial t)]^2$ and neglect the second time derivative. We work at resonance with the unperturbed plasma, i.e., $\omega^2 = 4\pi n_0 e^2/m_e$ and let ω_{pe}^2 depend on the actual density which may be different from n_0 because of the excitation of low-frequency perturbations. Assuming quasi-neutrality, we then readily obtain the dimensional form of (24a). It is coupled through the right-hand side with the ion motion given by (24b, c). In the equation of motion (24c) the low frequency electric potential has been replaced by an expression which satisfies the electron momentum equation averaged over one plasma period $2\pi/\omega$

$$\frac{d}{dx}|v_0|^2 = \frac{e}{m_e}\frac{d\phi_s}{dx} - \frac{1}{m_e n_s}\frac{dp_s}{dx} \tag{27}$$

Equation (27) is analogous to eq. (1d) and includes the action of the hf waves on the slow electron motion. Here, v_0 is the amplitude of the rapid oscillating electron velocity ($v_e = v_0\, e^{-i\omega t} +$ c.c.) and is related to $E_0(x, t)$ by

$$v_0 = \frac{eE_0}{im_e\omega} \tag{28}$$

We also assume an isothermal equation of state for the slowly varying pressure: $p_s = n_s \kappa T_e$, $T_e = \text{const.}$ (subscript s denotes slowly varying quantities). Deviations from the isothermal law, like the generalized equation of state (14) of the previous chapter, can easily be incorporated in (27) [24].

We now look for the stationary solutions of (24) in the form

$$E(x, t) = w(x - Mt) \exp\{i[\theta(t) + \Gamma(x)]\} \tag{29a}$$

$$n_i(x, t) = n(x - Mt) \tag{29b}$$

$$u_i(x, t) = u(x - Mt) + M \tag{29c}$$

Substituting (29) in (24) we get from the imaginary part of (24a)

$$\Gamma(x) = \epsilon M x/3 \tag{30}$$

The real part gives

$$3w_{xx} = (n + A - 1)w \tag{31}$$

where the nonlinear frequency shift A is

$$A = 2\epsilon\theta_t + \epsilon^2 M^2/3 \quad \text{(subscript means differentiation)} \tag{32}$$

The integrated ion equations now become

$$nu = -M \tag{33a}$$

$$\frac{u^2}{2} + \ln n + w = M^2/2 \tag{33b}$$

where we used an unperturbed state at infinity ($n = 1, u = -M$) as boundary conditions, corresponding to a localized solution we are looking for. The last two equations are combined to yield

$$w^2 = M^2(1 - n^{-2})/2 - \ln n \tag{34}$$

Using this relation we integrate eq. (31) once and find

$$3w_x^2 + (1 - A)w^2 + n(1 + M^2/n^2) = 1 + M^2 \tag{35}$$

where the boundary conditions are again used.

We now look for a solitary wave solution centered at the origin, i.e., a bell shape for the electric field quantity w and an inverted bell shape for density n, which turns out to be always less than unity (density dip). Accordingly, we let $W = w(0)$ to be the maximum of $w(x)$, and $N = n(0)$ to be the minimum of n. The nonlinear dispersion relation, evaluated from (34) at $x - Mt = 0$, now becomes

$$M^2 = 2(W^2 + \ln N)/(1 - N^{-2}) \tag{36}$$

Note, that the limiting case $W^2 = 0$ does not directly lead to the dispersion relation (8) of ion acoustic solitons (with $p_e(\psi) = n_e(\psi) = e^{\psi}$) because quasi-neutrality was used in deriving (36). We will return back to this point later.

The frequency shift A is obtained from eq. (35) by setting $w_x = 0$, at $w = W$, and $n = N$

$$A = 1 + (N - 1)(1 - M^2/N)W^{-2} \tag{37}$$

Using (34) we can rewrite (35) in terms of n_x and n to obtain the analog to eq. (6)

$$n_x^2/2 + V(n; N, W) = 0 \tag{38}$$

We have included N and W in the argument of V to indicate that the solution depends on two independent parameters. The "potential energy" is given by

$$V(n; N, W) = \frac{2n^2w^2}{3(1 - M^2/n^2)^2}\left[(1 - A)w^2 + (n - 1)(1 - M^2/n)\right] \tag{39}$$

where w^2 is related to n by eq. (34).

To see whether (38) admits soliton solutions, we expand V around $n = N$ and $n = 1$ (note, that it holds $N \leqslant n \leqslant 1$), and obtain

$$V(n; N, W) = \begin{cases} \dfrac{2N^2W^2}{3(1 - M^2/N^2)}\left[1 - \dfrac{1 - N}{NW^2}\left(1 - \dfrac{M^2}{N}\right)\right](n - N) & n - N \ll 1 \\ -2A(1 - n)^2/3 & 1 - n \ll 1 \end{cases} \tag{40}$$

Thus V behaves properly at the boundaries and represents solitons if it is negative in the range $N < n < 1$. This gives the condition $N^2 > M^2$ from which $A > 0$ follows. The frequency shift of the hf waves $\delta\omega = -(A/2)\omega$ is always negative. The region outside the density trough is, therefore, overdense for the waves, which are localized at the underdense cavity region.

The range of existence of the two parametric solitons is shown in Fig: 4. It lies between the two curves labelled $M = 0$ and $M = N$. Also curves of constant Machnumber are plotted in the $W^2, \delta N$ plane ($\delta N = 1 - N$). From this diagram we can draw two interesting conclusions:

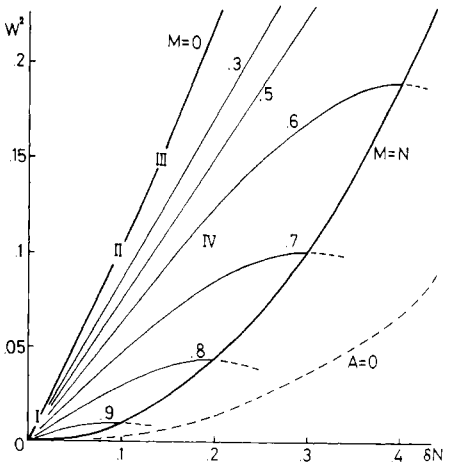

Fig. 4. The existence region of Langmuir solitons. Here, $W^2 = |E|^2_{MAX}/4\pi n_0 \kappa T_e$ and $\delta N = 1 - N$, where $N = n_{MIN}/n_0$. Also lines of the constant Machnumber are plotted. Solitons can exist between the lines $M = 0$ and $M = N$. The dashed line marks a vanishing frequency shift which is negative above the line. The Roman numbers represent experimental data.

(1) The more field is trapped in a given density trough, the slower the soliton moves.

(2) High speed ($M \lesssim 1$) solitons have necessarily small amplitudes.

It follows that the adiabatic ($M = 0$) soliton has the largest amount of trapped field. Hence, the hf field trapped in the density trough hinders the motion of the soliton, similar to the retarding effect of trapped particles in an ion acoustic soliton.

No soliton of the type assume above exists for values of W^2 and δN lying below the line $M = N$. As we will see, near this line the assumption of quasi-neutrality is violated, and a new type of soliton appears.

3.2. *Small amplitude Langmuir solitons*

We now derive the small amplitude limit by letting

$$(\delta N)^2 \ll W^2 \leqslant \delta N \ll 1 \tag{41}$$

We obtain by Taylor-expansion

$$M^2 = 1 - W^2/\delta N - \delta N\left(1 - \frac{3}{2}\frac{W^2}{\delta N}\right) \tag{42}$$

$$A = \frac{\delta N}{2}\left[1 + \frac{\delta N}{2}\left(1 - \frac{2}{3}\frac{\delta N}{W^2}\right)\right] \tag{43}$$

and the classical potential energy becomes

$$V(\delta\hat{n}; \delta N, W^2) = -\frac{\delta\hat{n}^2}{3}(\delta N - \delta\hat{n}) \tag{44}$$

where $\delta\hat{n} = 1 - n$.

It follows that

$$\delta\hat{n} = \delta N \operatorname{sech}^2\left[\left(\frac{\delta N}{6}\right)^{1/2}(x - Mt)\right] \tag{45a}$$

$$w^2 = W^2 \operatorname{sech}^2\left[\left(\frac{\delta N}{6}\right)^{1/2}(x - Mt)\right] \tag{45b}$$

and

$$\theta(t) = \frac{1}{2\epsilon}\left(A - \frac{\epsilon^2 M^2}{3}\right)t \tag{46}$$

The solution for the real electric field in dimensional form becomes

$$\frac{E(x,t)}{(16\pi n_0 \kappa T_e)^{1/2}} = W \operatorname{sech}\left(\frac{x - v_g t}{L}\right) \cos(kx - \omega_k t) \tag{47}$$

where the group velocity v_g, the soliton width L, the wave number k and frequency ω_k of the internal oscillation are given by

$$L = (6/\delta N)^{1/2}\lambda_D; \quad v_g = Mc_s; \quad k\lambda_D = \epsilon M/3 \tag{48a}$$

$$\omega_k^2 = \omega^2[1 + 3(k\lambda_D)^2 - \delta N/2 + O(\delta N^2)] \tag{48b}$$

The frequency relation shows that the hf wave packet is composed on Langmuir waves ($\omega^2 = 4\pi n_0 e^2/m_e$) which are, however, frequency-downshifted due to the presence of the density dip. The effective density for these waves is $n_0(1 - \delta N/2)$. The waves can, therefore, only exist in the cavity and are evanescent outside. This is expressed by the sech profile.

The soliton (45) satisfies

$$2i\epsilon \frac{\partial}{\partial t} E + 3 \frac{\partial^2}{\partial x^2} E = \delta n E \tag{49a}$$

$$\left(\frac{\partial^2}{\partial t^2} - \frac{\partial^2}{\partial x^2}\right)\delta n = \frac{\partial^2}{\partial x^2}|E|^2 \tag{49b}$$

where $\delta n = -\delta \hat{n}$. The ion equations (24b, c) reduce in the small amplitude limit to the wave equation of ion acoustic waves in the infinite wave-length limit, driven by the ponderomotive force.

Depending on the relative strength of $W^2/\delta N$, the soliton (45) represents

(i) the soliton of Rudakov [25] if $\delta N^2 \ll W^2 \lesssim \delta N \ll 1$ and

(ii) the soliton of Karpman [26] if $\delta N^2 \ll W^2 \ll \delta N \ll 1$.

The sonic soliton of Karpman, e.g., prevails if $W^2 = O(\delta N^{3/2})$. Its velocity, $M^2 = 1 - O(\delta N^{1/2})$, lies above the critical line $M^2 = N^2 = 1 - \delta N$ in Fig. 4. If we lower W^2 further, so that $W^2 = O(\delta N^2)$, we pass the line $M^2 = 1 - \delta N$, and the above theory breaks down. The reason is that terms in the ion equation, neglected up to now, become of the same order than the retained ones and must be kept. These are the lowest order nonlinear term and the dispersion term, so that instead of (49b) we get

$$\left(\frac{\partial^2}{\partial t^2} - \frac{\partial^2}{\partial x^2}\right)\delta n = \frac{\partial^2}{\partial x^2}\left[|E|^2 + \delta n^2 + \frac{\partial^2}{\partial x^2}\delta n\right] \tag{50}$$

Soliton solutions of the system (49a), (50) have been found by Makhankov [27] and Nishikawa et al. [28] and read

$$\delta n = -\delta N \operatorname{sech}^2[z] \tag{51a}$$

$$E = -\frac{2\delta N}{3^{1/2}} \operatorname{sech}[z] \tanh[z] \exp[i(\theta(t) + \Gamma(x))] \tag{51b}$$

where

$$z = (\delta N/18)^{1/2}(x - Mt); \quad M = 1 - 5\delta N/9;$$

$$\theta(t) = \delta N t/(12\epsilon); \quad \Gamma(x) = \epsilon M x/3$$

This is a one-parametric family of solitons, distinguished by a node of the electric field at the center. In the language of quantum mechanics this soliton represents the first excited state whereas the former soliton can be considered as the ground state. Note, that for this soliton $M^2 = 1 - \frac{10}{9}\delta N < M^2 = N^2 \simeq 1 - \delta N$.

Let us close this section by describing the three-parametric soliton which arises if deviations of the isothermal equation of state for the electrons are taken into account [24]. These lead to an ion equation of the form

$$\left(\frac{\partial^2}{\partial t^2} - \frac{\partial^2}{\partial x^2}\right)\delta n = \frac{\partial^2}{\partial x^2}\left[|E|^2 - \frac{4b}{3}\{\delta N^{3/2} - (\delta N + \delta n)^{3/2}\}\right] \tag{52}$$

where the electron trapping parameter b is again given by formula (17).

It can be shown that soliton solutions of the system (49a), (52) exist if

$$\rho^{-1} \equiv \frac{4b}{3}\frac{\delta N^{3/2}}{W^2} < 1 \tag{53}$$

This condition sets an upper bound for the trapping parameter b. The Mach-number is given by

$$M = 1 - \frac{W^2}{2\delta N}(1 - \rho^{-1}) \tag{54}$$

Analytic explicit solutions of the soliton exist only in special cases. For $\rho^{-1} = 2/3$, we find

$$\delta n = -\delta N[1 - 4\sinh^2(z)\exp(-2z)] \tag{55a}$$

$$|E| = W \exp(-z)[(2 - \exp(-2z))(1 - \tfrac{8}{3}\sinh^2(z))]^{1/2} \tag{55b}$$

where

$$z = 0.32\delta N^{1/2}|x - Mt|$$

In the isothermal limit $\rho^{-1} \to 0$ the three-parametric soliton reduces to that obtained by Karpman.

3.3. *Langmuir-solitons in experiments*

Now we compare our analytical results with existing experiments. For envelope solitons in order to exist we note that two basic requirements have to be satisfied. Firstly, there must be a source of hf Langmuir waves. This can be an electron beam which excites Langmuir waves via the two-stream instability, an electric field at resonance applied externally in a capacitor experiment, or the mechanism of linear mode conversion of electromagnetic waves into Langmuir waves at the resonance layer of an inhomogeneous plasma. Secondly, the processes which may destroy soliton formation have to be weak or balanced by additional arrangements. Damping, linear and nonlinear instability of a soliton, multidimensionality and plasma-nonuniformity causing wave convection and acceleration are examples. Last not least, there enters the problem of the accessibility and the development of the soliton leading to a stationary state.

Before mentioning the experimental results, we present some ideas how a soliton can be formed from an initially unperturbed state. As an example, we consider an electron beam penetrating an unmagnetized plasma [29]. For a cold and relativistic beam, the collective modes follow the linear dispersion relation

$$1 - \omega_{pe}^2/\omega^2 - \omega_b^2/[\gamma_0^3(\omega - kv_0)^2] = 0 \tag{56}$$

where v_0 is the beam velocity, $\omega_b^2 = 4\pi n_b e^2/m_e$ with n_b being the beam density and $\gamma_0 = (1 - v_0^2/c^2)^{-1/2}$ is the relativistic factor. Equation (56) has unstable solutions, the fastest growing mode is given by

$$\omega = \omega_{pe}[1 - (\mu/2)(1 - 3^{1/2}i)]; \quad k_0 = \omega_{pe}/v_0 \tag{57}$$

where $\mu = \gamma_0^{-1}(n_b/2n_0)^{1/3}$ is assumed to be small. Nonlinear effects such as the trapping of beam particles, halt the growth, and an oscillatory state of the wave amplitude sets in, which is described by the well-known SINGLE WAVE MODEL [30, 31]. This state is characterized by the motion of trapped electrons sloshing back and forth in the potential well of the wave. In the

average the single mode has a frequency below the electron plasma frequency. This mode acts like a pump and excites hf sidebands and ion oscillations via the oscillating two-stream instability OTSI [32]. Numerical solutions [33] of the coupled system consisting of the single wave model and the sidebands show a hydrodynamic decoupling of the beam at later times. The beam which has gained a finite thermal spread only weakly interacts with the excited waves. In the final stage, the waves representing a finite energy content produce through mode coupling process higher harmonics and approach an ensemble of solitons. This strong turbulence phenomenon is not restricted to the cold beam approximation and occurs under wide conditions for warm beams as well [34].

In a series of experiments performed in a double plasma device at the UCLA, Wong and Quon [35] distinguished three different cases for the development of the system depending on the beam strength with typical values $n_b/n_0 \sim 0.05$–0.1 and $v_0/v_{te} \sim 5$–10. For a weak beam, the maximum amplitude of the beam mode was below the threshold of OTSI, and hence no modulation was observed. For values just above the threshold, the parametric process set in and an ion wave with $k = 2k_0$ grew. What follows, is wave trapping in the density troughs and a chain of soliton-like structures which became stationary after several ion plasma periods. For a stronger beam, the development was essentially the same except that the localized structures had finally larger amplitudes and their formation time was shorter. Three cases of stationary solitons were observed with properties (i) they were not propagating in space and (ii) the normalized maximum field in each of them was nearly equal to the normalized depth of the cavity. When plotted in the existence diagram Fig. 4, labelled by I, II, III, these values lie exactly on the curve for a non-propagating, i.e., $M = 0$, soliton.

On the other hand, in the experiments of Ikezi et al. [36], an ion acoustic test wave was launched and the density modification by switching on the beam was studied. The result was a chain of stationary localized structures moving with $v_g = 0.6c_s$. The values $W^2 = |E_{MAX}|^2/4\pi n_0 \kappa T_e$ and $\delta N = |\delta n_{MIN}|/n_0$ of these structures lie on the curve $M = 0.6$ in Fig. 4, identifying them as solitons. In this experiment, the stationarity was supported by the presence of the beam which balanced the loss of the field energy perpendicular to the beam direction. When the beam was switched off, the field diminished whereas the density cavities were longer stable and attained higher speed. This corresponds to the motion of a point in the existence diagram (Fig. 4) on a vertical line downward. Hence, as stated before, the trapped field corresponds to the "mass of a particle" which increases its speed when mass is lost.

Finally, standing spikes were also observed in the capacitor experiments of Kim et al. [37] at the resonance layer of an inhomogeneous plasma. The observed values at saturation $W^2 = 0.26$ and $\delta N = 0.25$, not plotted in Fig. 4, again satisfy the Mach-number relation (36) of a standing soliton. In this strong field case, the soliton is not strictly stationary, but breaks up later on into isolated components which propagate down the density gradient carrying the density cavity with it. This corresponds to the studies of soliton propagation on linear density profiles [38–40], in which a similar behaviour is found.

Although in most of the experiments the one-dimensionality is not well established, the observed localized structures carry the properties of Langmuir solitons so that we may identify them. The interpretation is as follows: Through the beam or the density gradient a preferred direction is given where soliton formation takes place. If an excess of wave energy, compared to $W^2 \approx \delta N$ is present, it can be convected away into the perpendicular direction and/or balances the loss of energy due to wave damping. This might explain the tendency towards one-dimensional solitons, although the physics involved is inherently three-dimensional.

Furthermore, one can also restrict the sytem to evolve only in one-dimension. This is achieved, e.g., by applying an external magnetic field in the plasma [41] or by using devices with large cross dimensions. In this case, it turns out that an abundant wave energy cannot be convected away effectively, and the evolution of the system basically becomes time dependent. Such a process is investigated next.

4. Miscellaneous

Here we discuss a transient phenomenon which we refer to as soliton flash. Furthermore, we present an example to show how stationary solitons can be used to test the accuracy of numerical schemes in the nonlinear regime.

4.1. *The soliton flash*

Following the idea expressed at the end of the previous section, we extend the coupled system (49) in three ways [42–44]:

(1) Include an external driver in the Schrödinger equation (49a). It may represent an electron beam or the transverse magnetic field of a p-polarized wave, obliquely incident onto an inhomogeneous plasma.

(2) Take into account various damping processes, e.g., Landau-collisional as well as damping originating from nonlinear effects in both equations (49a, b).

(3) Describe the linear low-frequency response correctly by making use of the correct dispersion relation of the ion-acoustic waves.

These generalizations are best formulated in Fourier space. Let $\hat{E}(k, t)$ and $\delta\hat{n}(k, t)$ be the Fourier transform of $E(x, t)$ and $\delta n(x, t)$, then we define the following collective variables

$$a(k,t) = \frac{-i\hat{E}(k,t)\omega_k^L}{(2\pi n_0 \kappa T_e)^{1/2}\omega_{pe}} \tag{58a}$$

$$b(k,t) = \frac{\omega_k^s \delta\hat{n}(k,t)/n_0 + i(\partial/\partial t)\delta\hat{n}(k,t)/n_0}{2^{1/2}|kc_s|} \tag{58b}$$

where ω_k^L and ω_k^s are the Bohm–Gross frequency and ion acoustic frequency, respectively,

$$\omega_k^L = \omega_{pe}(1 + 3(k\lambda_D)^2)^{1/2} \tag{59a}$$

$$\omega_k^s = |kc_s|(1 + (k\lambda_D)^2)^{-1/2} \tag{59b}$$

Using Hamiltonian formalism described in [42], we obtain the following set of coupled mode equations [43]:

$$\frac{\partial}{\partial t}a(k,t) = -i[\tfrac{3}{2}(k\lambda_D)^2\omega_{pe} - i\gamma_k]a(k,t)$$
$$-i2^{-3/2}\omega_k^L \sum_{\substack{k_2,k_3 \\ k_2+k_3=k}} [b(k_2,t) + b(-k_2,t)^*]a(k_3,t)$$
$$-\frac{|E_{ext}|}{(8\pi n_0 \kappa T_e)^{1/2}}\omega_{pe}\exp(-i\delta\omega t)\delta_{k,0} \tag{60a}$$

$$\frac{\partial}{\partial t}b(k,t) = -i[\omega_k^s - i\Gamma_k]b(k,t)$$
$$-i2^{-3/2}\omega_k^s \sum_{k_2,k_3} a(k_2,t)a(-k_3,t)^*\delta_{k_2+k_3,k} \tag{60b}$$

where γ_k and Γ_k are appropriately chosen damping rates [44], and $\delta\omega = \omega_0 - \omega_{pe}$, where ω_0 is the frequency of the external pump. For resonance absorption, $\delta\omega$ vanishes at the resonance point and $E_{ext} = B(x_c)\sin\theta_0$, where $B(x_c)$ is the magnetic field of the transverse wave at the critical density, and θ_0 is the angle of incidence.

For a moment let us neglect dissipation and transform the equations back into real space, so we have

$$\left(\mathrm{i}\frac{\partial}{\partial t} + \tfrac{3}{2}\omega_{pe}\lambda_D^2\frac{\partial^2}{\partial x^2}\right)E = \frac{\omega_{pe}}{2}\left[\left(1 - \tfrac{3}{2}\lambda_D^2\frac{\partial^2}{\partial x^2}\right)\frac{\delta n}{n_0}E + E_{ext}\,\mathrm{e}^{-\mathrm{i}\delta\omega t}\right] \tag{61a}$$

$$\left(1 - \lambda_D^2\frac{\partial^2}{\partial x^2}\right)\left(\frac{\partial^2}{\partial t^2} - c_s^2\frac{\partial^2}{\partial x^2}\right)\frac{\delta n}{n_0} = c_s^2\frac{\partial^2}{\partial x^2} \times \left[\frac{|E|^2}{4\pi n_0 \kappa T_e} + \lambda_D^2\frac{\partial^2}{\partial x^2}\frac{\delta n}{n_0}\right] \tag{61b}$$

from which the extensions with respect to (49) become obvious.

Using the numerical algorithm, described in more detail in the second part of this section, we solve the full system (60) numerically. We apply an external field $|E_{ext}|^2/4\pi n_0\kappa T_e = 10^{-3}$ during the interval $0 \leqslant \omega_{pi}t \leqslant 13.5$ and $\delta\omega = -2\omega_{pi}$. The solution is displayed in Figs. 5 and 6. The graphs exhibit the spatial dependence of the normalized field intensity and ion density perturbation at equidistant time steps. We recognize the electric field to be localized in space and time. The field intensity strongly overshoots the value of a stationary soliton for given δN at $\omega_{pi}t = 14$ and decays rapidly afterwards. Here, the decay is enforced by switching off the pump. We note, that this overshooting is, to a lesser extent, also observable for a continuous pump injection. Although a numerical instability produced by the strong field cannot be excluded, the observation of this phenomenon in laboratory experiments and particle simulations proves, as shown later, that it is realistic. It is called soliton flash to remind of the shape of transient state of the wave packet.

On the other hand, the density pattern shows at the right place the cavity with density barriers on both sides. This perturbation is standing and growing as long as field trapping occurs.

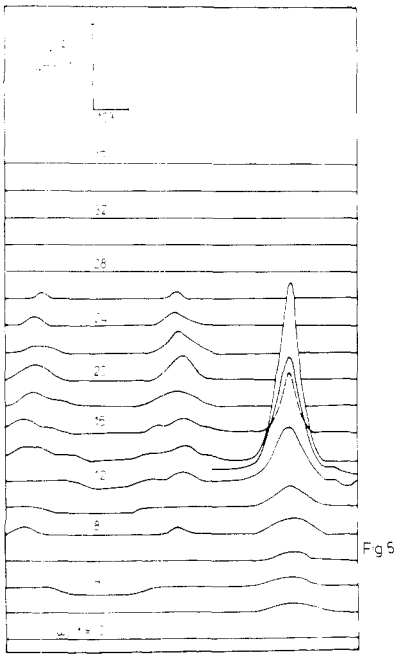

Fig. 5. The space–time history of the normalized field intensity.

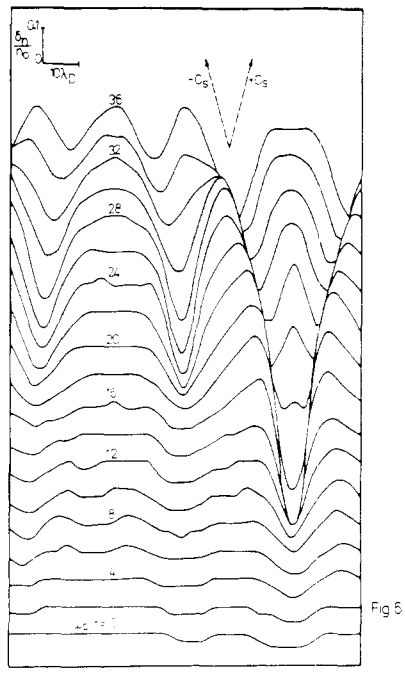

Fig. 6. The space–time history of the ion density perturbation corresponding to Fig. 5.

However, after the field has dropped to a small value, the cavity splits into two streamers propagating apart with ion acoustic velocity.

This feature can easily be understood in terms of the driven ion wave equation. Approximating the normalized electric field by a Gaussian profile [45],

$$|E|^2 = W^2\exp\left[-\left(\frac{x^2}{x_0^2} + \frac{t^2}{t_0^2}\right)\right] \tag{62}$$

which corresponds to Fig. 5, we can solve the ion equation (49b). A particular solution is given by

$$\delta n(x,t) = \frac{1}{2}\int_{t_i}^{t} \mathrm{d}\tau \int_{z-(t-\tau)}^{z+(t-\tau)} \mathrm{d}\xi\,\frac{\partial^2}{\partial\xi^2}|E(\xi,\tau)|^2 \tag{63}$$

where t_i lies in the remote past where the perturbations are negligible. Inserting (62) in (63) and changing the order of integration, after some algebra one finds

$$\delta n(x,t) = \sigma^{-2}W^2\left[-\exp\left(-x^2/x_0^2 - t^2/t_0^2\right) + \frac{x_0\pi^{1/2}}{2\sigma t_0^2}\sum_{\pm}\pm(x \mp t) \times \exp\left[-(x \mp t)^2/(\sigma t_0)^2\right]\operatorname{erfc}\left\{\left(\mp x - \frac{x_0^2}{t_0^2}t\right)\Big/(\sigma x_0)\right\}\right] \tag{64}$$

where $\sigma^2 = (1 + x_0^2/t_0^2)$.

The first term on the right hand side of (64) describes the cavity which appears at $x = 0$ with maximum depth at $t = 0$. Note, that the maximum of $|E|^2$ expressed in terms of δN, namely $|E|^2_{MAX} = \sigma^2\delta N$ exceeds $|E|^2_{MAX} = \delta N$, the corresponding quantity for a stationary standing (adiabatic) soliton. The second term represents the left and right propagating streamers depending on the sign. They move with ion sound speed and have the form of a leading density hump followed by a density dip as in Fig. 6. These streamers carry the information about the actual field and allow to estimate the strength W and widths x_0 and t_0 of the field by measuring the maximum density perturbation and the distance between both extrema of a streamer.

Experimentally, the overshooting of $|E|^2$ and the related

streamers are evident in the microwave experiments of Wong and collaborators as summarized in [46]. This is especially seen in Figs. 7, 8 and 11 of that paper (see also [47]). The conditions for the occurrence of a flash-like behaviour of the total electric field, together with the splitting of the cavity in these resonance adsorption experiments are a gentle density gradient ($k_D L > 500$; L is the density scale length and $k_D = \lambda_D^{-1}$) and a pump duration of $\omega_{pi} t \lesssim 50$. It is worthy to mention that the streamers produced in a non-uniform plasma propagate subsonic (supersonic) up (down) the density profile. The reason is a plasma drift which is due to an acceleration of the plasma towards the vacuum by the ambipolar field, and which superimposes on the streamer motion. We mention that computer experiments [48–50] have also revealed the ingredients of the soliton flash and the induced development of cavities.

Finally, the soliton flash is expected to occur at the initial stage of profile modification in laser driven fusion when the density scale length exceeds the vacuum wave length λ_0. The perpendicular extension of the laser beam will be much larger than λ_0, so that the system will evolve more or less one-dimensional and give rise to non-stationary plasma behaviour, as discussed here.

4.2. *Solitons in numerical experiments*

Nonlinear wave equations which possess exact solutions are good candidates to check various kinds of numerical algorithms. The KdV-equation and the Burgers equation which admit soliton and shock-like solutions, respectively, are examples and widely used in this respect.

The work of Arakawa [51] demonstrates that finite difference schemes could be valuable, provided nonlinear equations are written in a conservative form. Several attempts were made to reduce phase errors which originate from the discretization of space derivatives [52–60]. These phase errors can be minimized or even eliminated if space derivatives are treated exactly by means of Fast Fourier Transform techniques (FFT). The latter are now generally available in subroutine form. An example is the split-time Fourier method [61–63]. Here, in the first step the nonlinear convective term is treated by means of finite difference approximation, and in the second step the linear terms are handled by means of FFT. A further example is the Accurate Spatial Derivative method (ASD) [63, 64], where a Taylor expansion is used to perform the time stepping, and for the remaining calculations FFT is applied. Treating nonlinear terms (or linear terms with variable coefficients) by FFT means, that one faces with the problem of aliasing interactions or, what is equivalent, with the distinction between spectral (SM) and pseudo-spectral (PSM) method [65–67].

In this last section, we report on numerical experiments in connection with soliton propagation in which both methods, SM and PSM, are further analyzed [68, 69]. Firstly, we discuss the origin of aliasing interactions and then present the numerical results.

In one dimension finite discrete Fourier transformation is defined by the transformation pair

$$u(x) = \sum_{k \in B_K} \tilde{u}(k) \exp(ikx) \qquad x \in B_x$$

$$\tilde{u}(k) = N^{-1} \sum_{x \in B_x} u(x) \exp(-ikx) \qquad k \in B_K \tag{65}$$

where

$$B_x = \{x \mid x = n/N \quad 0 \leqslant n < N\}$$

$$B_K = \{k \mid k = 2\pi m \quad -K \leqslant m < K\} \tag{66}$$

and $2K = N$, n and m are integers. It has the orthogonality relation

$$N^{-1} \sum_{x \in B_x} \exp(ikx) = \delta_{k, 2\pi eN} \tag{67}$$

instead of $\delta_{k,0}$ for infinite Fourier transformation. Here δ is the Kronecker symbol and $e = 0, \pm 1, \pm 2, \ldots$. From this property it follows that the Fourier transform of the local product $F(x) = u(x)v(x)$, which stands, e.g., for hydrodynamic nonlinearities, becomes

$$\tilde{F}(k) = \sum_{p,q} \tilde{u}(p)\tilde{v}(q)\delta_{p+q-k,0} + \sum_{p,q,e=\pm 1} \tilde{u}(p)\tilde{v}(q)\delta_{p+q-k,2\pi eN} \tag{68}$$

where $k, p, q \in B_K$. In the convolution sum the last term represents the aliasing interactions resulting from the inability of the grid point values to distinghish between the wave number k and its aliases $k + 2\pi eN$. How these additional terms enter will become apparent shortly.

Let us consider the KdV–Burgers' equation

$$\frac{\partial}{\partial t}\phi + (1 + \phi)\frac{\partial \phi}{\partial x} - \frac{\nu}{2}\frac{\partial^2 \phi}{\partial x^2} + \frac{1}{2}\frac{\partial^3 \phi}{\partial x^3} = 0 \tag{69}$$

and its second order equivalent

$$\frac{\partial^2 \phi}{\partial t^2} - \frac{\partial^2}{\partial x^2}(\phi + \phi^2) - \nu \frac{\partial^2}{\partial x^2}\phi - \frac{\partial^4}{\partial x^4}\phi = 0 \tag{70}$$

where ν is a constant viscosity, and solve the corresponding Fourier equations. In periodic systems, as mentioned before, this is the best way to represent the various derivatives. For both equations the Fourier transformed version can be written as

$$\frac{\partial}{\partial t} C_k = -i\omega_k \left(C_k + \frac{1}{2} \sum_{p,q} v_{-k,p,q} C_p C_q \right) + D_k \tag{71}$$

where C_k is the Fourier transform of ϕ

$$\phi(x, t) = \sum_{k=-\infty}^{+\infty} C_k(t) \exp(ikx) \tag{72}$$

and the expressions for ω_k, $v_{-k,p,q}$ and D_k are given in [69]. The matrix element $v_{-k,p,q}$ is thereby proportional to $\delta_{-k+p+q,0}$. Introducing a cut-off in the Fourier-space, $|k| \leqslant 2\pi K$, the calculation of the convolution sum would demand N^2 (N^{2d} in d-dimensions) operations instead of N (N^d) operations if the calculations were performed in real space. One circumvents this ineffective procedure by transforming back into real space, performing there the local product and by returning then to k-space. Using FFT methods the number of operations is, thereby, reduced to the order of $rN^d \log_2 N^d$, where r is the number of Fourier transformations involved. In the last step, however, the aliasing terms appear and introduce additional terms in the truncated version of (71). If these terms are not eliminated, the corresponding numerical algorithm will be called pseudospectral method (PSM), otherwise one refers to SM. In the latter, additional shifted grids, corresponding to a *nonlocal* representation of the nonlinear term, provide an elimination procedure [70], whereas the PSM uses the local representation directly and is, therefore, also referred to as collocation method.

Clearly, PSM is simpler and less time consuming, and the question arises whether the dealiasing procedure is necessary. Our answer will be in favour of SM. We follow the soliton solution ($\nu = 0$) in time

$$\phi(x,t) = \phi_0 + \psi \operatorname{sech}^2[(\psi/6)^{1/2}(x - Mt)] \tag{73}$$

$$M = \begin{cases} 1 + \phi_0 + \psi/3 & \text{for eq. (69)} \\ (1 + 2\phi_0 + 2\psi/3)^{1/2} & \text{for eq. (70)} \end{cases}$$

and compare the result with the analytic solution (73). As an additional check, we also calculate the first three invariants of (69), respectively (71), which in the continuous version, are

$$I_1 = \int \mathrm{d}x\, \phi(x,t) = C_0(t)$$

$$I_2 = \int \mathrm{d}x\, \phi^2(x,t) = \sum_k |C_k(t)|^2$$

$$I_3 = \int \mathrm{d}x \left[\phi^3/3 - \left(\frac{\partial\phi}{\partial x}\right)^2 \Big/ 2\right]$$

$$= \frac{1}{3} \sum_{k_1,k_2,k_3} C_{k_1} C_{k_2} C_{k_3} \delta_{k_1+k_2+k_3,0} - \frac{1}{2} \sum_k k^2 |C_k|^2 \tag{74}$$

In [69] it is shown that equivalent invariants exist also for the truncated forms of (71), provided the cut-off term is set to be zero. We have chosen ϕ_0 such that C_0 is zero for all times and the word invariant is meant in the sense of semi-conservation where the error made by time-differencing is disregarded.

Figure 7 shows the soliton with $\psi = 0.2$ after 125 ion plasma periods. Initially, it was centred at $X = -50$, so that it has moved once through the periodicity interval $0 \leqslant X < 100$ (from which only the right half is plotted). The solid curve, ϕ_{analyt}, is the analytical solution (73), the dotted curve, $\phi_{\text{num.1}}$, is obtained with the alias-free SM ($N = 64$), the dashed curve, $\phi_{\text{num.2}}$, is computed with PSM ($N = 64$), and the crosses denote the solution obtained by SM with half the number of Fourier modes ($N = 32$). We see that only the alias-free solutions agree with the analytical solution, whereas the PSM-solution deviates remarkably. The aliasing interactions *weaken* the nonlinearity, as seen by the decay of the original soliton into a smaller soliton and a dispersive ion acoustic wave packet. Note, that the delay of the PSM-soliton results from its smaller amplitude and is not related with linear phase errors which are absent here. Furthermore, if the number of grid points is halved ($N = 32$), SM still gives the correct answer. Thus, SM is much more accurate than

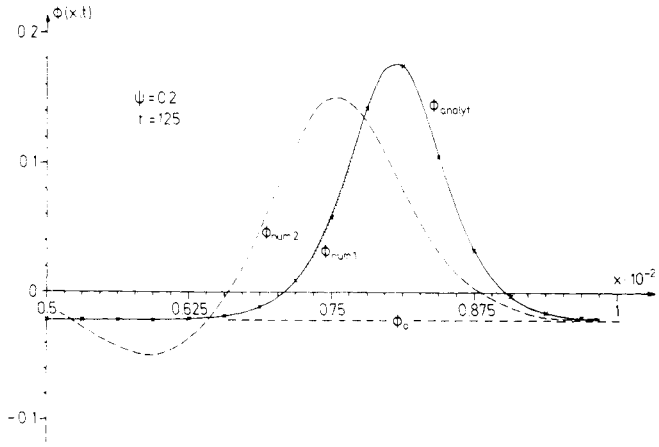

Fig. 7. The KdV-soliton as a function of space at $\omega_{pi}t = 125$. The solid curve, labelled ϕ_{analyt}, represents the analytical solution (73), the other curves are obtained numerically: the dotted curve, $\phi_{\text{num 1}}$, is calculated by means of the spectral method (SM), and the dashed curve, $\phi_{\text{num 2}}$, by means of the pseudo-spectral method (PSM), both with $N = 64$ Fourier-modes. Crosses denote the solution obtained by SM with $N = 32$.

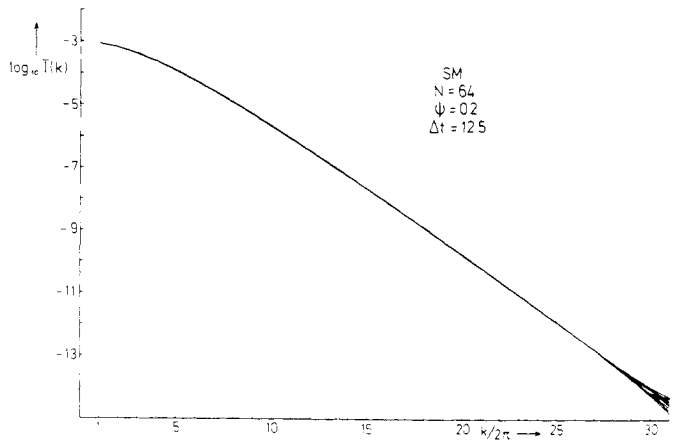

Fig. 8. The spectral energy density, $\bar{I}(k)$ vs. k at ten equidistant time steps ($\Delta\omega_{pi}t = 12.5$) calculated with SM ($N = 64$).

PSM with twice the number of modes. Since both need comparable computation time SM is, therefore, more efficient.

In all runs the invariants I_2, I_3 were conserved within a relative error of 0.2 per cent and $I_1 = C_0 = 0$ was conserved, since $\dot{C}_0 = 0$. This shows that the integral conservating property of a scheme does not automatically guarantee its accuracy.

In Fourier space the runs are seen in the next two figures where the spectral energy density $\bar{I}(k) = |C_k|^2 + |C_{-k}|^2$ is shown as a function of k at ten equidistant time steps ($\Delta t = 12.5$). Figure 8 is obtained by SM (64 modes) and Fig. 9 by PSM. Whereas in the former case the stationarity of the soliton is nearly perfect, its nonstationarity is obvious in the latter example. Note, that the spectrum at cut-off is ten orders of magnitude below the most energetic component. This shows that in the regime of low cut-offs and large computation times the dealiasing procedure cannot be avoided by including more modes. The deviation from the correct spectrum sets in at high wave numbers and propagates to lower values in the course of time.

Similar results are obtained with the smoothed sawtooth which is a nonstationary solution of Burgers' equation, and the results are not different if the Boussinesq-type equation (70) is used instead of (69).

We conclude with the remark that the aliasing interactions are false interactions and should be avoided for long term runs. In addition, the conservation of quadratic and higher order integral constraints which ensure the stability of a given scheme is not decisive for its accuracy.

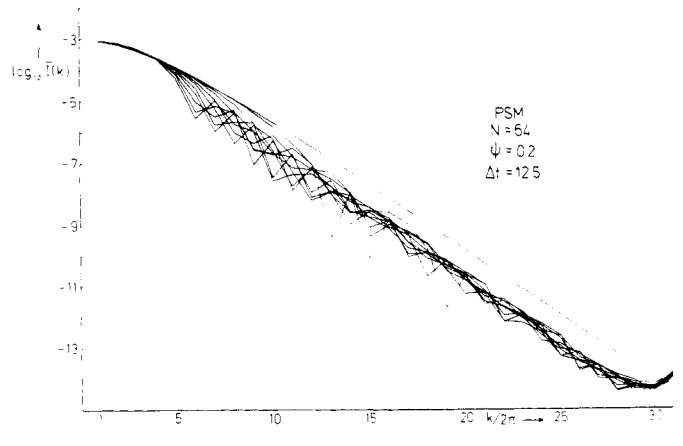

Fig. 9. The spectral energy density as a function of k at ten equidistant time steps performed with PSM ($N = 64$).

5. Summary

Trapped particles and waves have proven to play a key role in soliton behaviour because in a broad range both control the velocity and shape of solitons. Nonisothermal ion acoustic solitons with a smaller fraction of trapped electrons are found to move faster than the isothermal ones. However they are not yet explored experimentally. On the other hand, the localized structures consisting of Langmuir waves trapped in density cavities are observed in microwave- and beam experiments and seem to coincide with the theoretically predicted Langmuir solitons. For ion acoustic solitons the analysis was based on the time-independent equations where the non-linearities were taken into account completely. Stationary envelope solitons were constructed by making use of the full ion dynamics but neglecting electron nonlinearities. A non-stationary process has then been studied by including pump and dissipation in the coupled nonlinear Schrödinger-ion equation. If the system was allowed to evolve in one-dimension only, the hf wave energy passed a flash-like state and forced the cavity to split into streamers. Several experimental and numerical examples have shown to support this point of view on the development of a caviton. In numerical analysis, the study of soliton propagation turned out to be a excellent technique to check numerical algorithms. As an example, the pseudo-spectral method (collocation-method) was found to be erroneous in the nonlinear regime whereas the spectral method gives adequate results.

Of course, several problems in soliton theory such as stability, formation, other non-stationary processes, etc. were excluded in this article and definitely deserve more attention.

In summary, we have attempted to study specific aspects of soliton behaviour more explicitly, some of which are being overlooked occasionally in this attractive branch of nonlinear physics.

Acknowledgements

The author is grateful to Professor K. Elsässer and Drs. P. Shukla and M. Yu for their fruitful collaboration, the results of which are the basis for part of the present review. He also thanks Mrs. B. Malik for her commendable typing of this manuscript. This work was sponsored by the Sonderforschungsbereich Plasmaphysik Bochum/Jülich.

References

1. Jeffrey, A. and Kakutani, T., SIAM Rev. **14**, 582 (1972).
2. Scott, A. C., Chu, F. Y. F. and McLaughlin, D. W., Proceeding of the IEEE **61**, 1443 (1973).
3. Karpman, V. I., Nonlinear Waves in Dispersive Media, Pergamon Press, Oxford (1975).
4. Makhankov, V. G., Physics Reports **35**, C(1) 1–128 (1978).
5. Bernstein, I. B., Greene, J. M. and Kruskal, M. D., Phys. Rev. **108**, 546 (1957).
6. Schamel, H., J. Plasma Phys. **13**, 139 (1975).
7. Schamel, H., Plasma Phys. **14**, 905 (1972).
8. Sagdeev, R. Z., Rev. Plasma Phys. **4**, 23 (1966).
9. Forslund, D. W. and Freidberg, J. P., Phys. Rev. Lett. **27**, 1189 (1971).
10. Schamel, H., J. Plasma Phys. **9**, 377 (1973).
11. Zakharov, V. E. and Karpman, V. I., JETP **16**, 351 (1963).
12. Auerbach, S. P., Phys. Fluids **20**, 1836 (1977).
13. Morse, R. L. and Nielson, C. W., Phys. Rev. Lett. **23**, 1087 (1969).
14. Morse, R. L. and Nielson, C. W., Phys. Rev. Lett. **26**, 3 (1971).
15. Forslund, D. W. and Shonk, C. R., Phys. Rev. Lett. **25**, 1699 (1970).
16. Montgomery, M. D., Asbridge, J. R. and Bame, S. J., J. Geophys. Res. **75**, 1217 (1970).
17. Wong, A. Y., Quon, B. H. and Ripin, B. H., Phys. Rev. Lett. **30**, 1299 (1973).
18. Moiseev, S. S. and Sagdeev, R. Z., J. Nucl. Energy **C5**, 43 (1962).
19. Ichikawa, Y. H. and Watanabe, S., Journal de Physique, Colloque, C6-15 (1977).
20. Ikezi, H., Phys. Fluids **16**, 1668 (1973).
21. Means, R. W., Coroniti, F. V., Wong, A. Y. and White, R. B., Phys. Fluids **16**, 2304 (1973).
22. Zakharov, V. E., Sov. Phys.–JETP **35**, 908 (1972).
23. Schamel, H., Yu, M. Y. and Shukla, P. K., Phys. Fluids **20**, 1286 (1977).
24. Schamel, H. and Shukla, P. K., Phys. Rev. Lett. **36**, 968 (1976).
25. Rudakov, L. I., Sov. Phys.–Dokl. **17**, 1166 (1973).
26. Karpman, V. I., Plasma Phys. **13**, 477 (1971).
27. Makhankov, V. G., Phys. Lett. **A50**, 42 (1974).
28. Nishikawa, K., Hojo, H., Mima, K. and Ikezi, H., Phys. Rev. Lett. **33**, 148 (1974).
29. Schamel, H., Preprint 77-L 2-013, Ruhr-University Bochum, (1977, in German)
30. Onishchenko, I. N., Linetskii, A. P., Matsiborko, N. G., Shapiro, V. D. and Shevchenko, V. I., JETP Lett. **12**, 281 (1970).
31. O'Neill, T. M., Winfrey, J. H. and Malmberg, J. H., Phys. Fluids **14**, 1204 (1971).
32. Nishikawa, K., J. Phys. Soc. Japan **24**, 916 (1968) and **24**, 1152 (1968).
33. Schamel, H., Lee, Y. C. and Morales, G. J., Phys. Fluids **19**, 849 (1976).
34. Papadopoulos, K., Phys. Fluids **18**, 1769 (1975).
35. Wong, A. Y. and Quon, B. H., Phys. Rev. Lett. **34**, 1499 (1975).
36. Ikezi, H., Chang, R. P. H. and Stern, R. A., Phys. Rev. Lett. **36**, 1047 (1976).
37. Kim, H. C., Stenzel, R. L. and Wong, A. Y., Phys. Rev. Lett. **33**, 886 (1974).
38. Morales, G. J. and Lee, Y. C., Phys. Fluids **20**, 1135 (1977).
39. Chen, H. H. and Liu, C. S., Phys. Rev. Lett. **39**, 1147 (1977).
40. Shukla, P. K. and Spatschek, K. H., to appear in J. Plasma Phys. (1978).
41. Injeyan, H., Leung, P. L. and Wong, A. Y., Bull. Am. Phys. Soc. **21**, 1093 (1976).
42. Elsässer, K. and Schamel, H., J. Plasma Phys. **15**, 409 (1976).
43. Elsässer, K. and Schamel, H., Plasma Phys. **19**, 1055 (1977).
44. Schamel, H. and Elsässer, K., to be published (1978).
45. Peratt, A. L. and Watterson, R. L., Phys. Fluids **20**, 1911 (1977).
46. Wong, A. Y., in H. J. Schwarz and H. Hora (eds.), Laser Interaction and Related Plasma Phenomena, Vol. 4B, Plenum Press, New York and London (1977).
47. Wong, A. Y. and Stenzel, R. L., Phys. Rev. Lett. **34**, 727 (1975).
48. De Groot, J. S. and Tull, J. E., Phys. Fluids **18**, 672 (1975).
49. Sigov, Y. S. and Khodirev Y. V., Soviet Phys. Dokl. **21**, 444 (1976).
50. Pereira, N. R., Sudan, R. N. and Denavit, J., Phys. Fluids **20**, 936 (1977).
51. Arakawa, A., J. of Comp. Phys. **1**, 119 (1966).
52. Zabusky, N. J. and Kruskal, M. D., Phys. Rev. Lett. **15**, 240 (1965).
53. Pergrine, D. H., J. Fluid Mech. **25**, 321 (1966).
53. Vliegenthart, A. C., Journ. of Eng. Math. **5**, 137 (1971).
55. Johnson, R. S., J. Fluid Mech. **54**, 81 (1972).
56. Hammack, J. L., J. Fluid Mech. **60**, 769 (1973).
57. Eilbeck, J. C. and McGuire, G. R., J. Comp. Phys. **19**, 43 (1975).
58. Goda, K., J. Phys. Soc. Japan **39**, 229 (1975).
59. Greig, I. S. and Morris, J. LL., J. Comp. Phys. **20**, 64 (1976).
60. Eilbeck, J. C., and McGuire, G. R., J. Comp. Phys. **23**, 63 (1977).
61. Tappert, F. D., Invited Paper, Annual Meeting of the American Society, Las Vegas (1972).
62. Hardin, R. H. and Tappert, F. D., SIAM Rev. **15**, 423 (1973).
63. Gazdag, J., J. Comp. Phys. **13**, 100 (1973).
64. Canosa, J. and Gazdag, J., J. Comp. Phys. **23**, 393 (1977).
65. Orszag, S. A., J. Fluid Mech. **49**, 75 (1971).
66. Orszag, S. A., Studies in Appl. Math. **50**, 293 (1971).
67. Fox, D. G. and Orszag, S. A., J. Comp. Phys. **11**, 612 (1973).
68. Schamel, H. and Elsässer, K., Proc. of the 2nd European Conference on Computational Phys., Contributed Papers E 4, (1976).
69. Schamel, H. and Elsässer, K., J. Comp. Phys. **22**, 501 (1976).
70. Patterson, G. S. and Orszag, S. A., Phys. Fluids **14**, 2538 (1971).